Supplementary materials of "Revisiting the global budget of atmospheric glyoxal: updates on terrestrial and marine precursor emissions, chemistry, and impacts on atmospheric oxidation capacity"

Aoxing Zhang[1,2], Tzung-May Fu[1,2,3], Yuhang Wang[4], Enyu Xiong[1,2,5], Wenlu Wu[1,2,6], Yumin Li[7], Lei Zhu[1,2], Wei Tao[1,2], Kelley C. Wells[8], Dylan B. Millet[8], Zhe Wang[9], Bin Yuan[10], Min Shao[10], Christophe Lerot[11,12], Thomas Danckaert[11], Ruixiong Zhang[13], and Kelvin H. Bates[14]

[1]State Key Laboratory of Soil Pollution Control and Safety, Shenzhen Key Laboratory of Precision Measurement and Early Warning Technology for Urban Environmental Health Risks, School of Environmental Science and Engineering, Southern University of Science and Technology, Shenzhen, Guangdong 518055, China
[2]Guangdong Provincial Field Observation and Research Station for Coastal Atmosphere and Climate of the Greater Bay Area, Southern University of Science and Technology, Shenzhen, Guangdong 518055, China
[3]National Center for Applied Mathematics Shenzhen, Shenzhen, Guangdong 518055, China
[4]School of Earth and Atmospheric Sciences, Georgia Institute of Technology, Atlanta, GA, 30342, USA
[5]Department of Civil and Environmental Engineering, The Hong Kong Polytechnic University, SAR, Hong Kong, 999077, China
[6]Institute for Climate and Atmospheric Science, School of Earth and Environment, University of Leeds, Leeds LS2 9JT, U.K.
[7]Institute for Atmospheric and Climate Science, ETH Zurich, Zurich 8092, Switzerland
[8]Department of Soil, Water, and Climate, University of Minnesota, St Paul, MN 55108, USA
[9]Division of Environment and Sustainability, The Hong Kong University of Science and Technology, Hong Kong SAR, China
[10]Institute for Environmental and Climate Research, Jinan University, Guangzhou, Guangdong 511443, China
[11]Royal Belgian Institute for Space Aeronomy (BIRA-IASB), Brussels 1180, Belgium
[12]now at constellr S.A., Liège 4031, Belgium
[13]Atlassian US Inc., San Francisco, CA 94104, USA
[14]Department of Mechanical Engineering, University of Colorado Boulder, Boulder, CO 80309, USA

Correspondence: Tzung-May Fu (fuzm@sustech.edu.cn) and Yuhang Wang (yuhang.wang@eas.gatech.edu)

Note S1. Calculation of glyoxal yields using DSMACC

Our DSMACC simulations were set to the meteorological and chemical environments of a surface location in Southern China (Zou et al., 2023). The meteorological and chemical variables were fixed based on measurements from a field campaign in Hong Kong SAR, China (Xiong et al., 2025) : atmospheric surface pressure 1007 hPa; surface temperature 293 K; 5×10^3 ppm of H_2O (relative humidity of 22%), 0.7 ppm of CO, 40 ppb of O_3.

To constrain the production and concentration of OH in the model, two proxy compounds (named OHPRE and OHDECAY) were added in the mechanisms as a producer and consumer of OH. Under a typical NO_X concentration (1 ppb), we constrained a baseline OHPRE and OHDECAY to get a daily mean OH production rate of 1.3×10^6 molecules cm^{-3} s^{-1} with daily mean OH concentration of 1.6×10^6 molecules cm^{-3}. We conducted sensitivity simulations with NO concentrations ranging from 0.1 ppb to 5 ppb, assuming an ambient NO_2 to NO concentrations ratio of 4. At each NO_X sensitivity experiment, we preturb

OHPRE and OHDECAY by scale factors from 0.01 to 100, in order to cover real conditions of NO_X and OH concentrations in the atmosphere.

To quantify the glyoxal yields from different mechanisms, we constructed three distinct DSMACC models: D-MCM, D-GC, and D-GCnew. The D-MCM model incorporated the photochemical degradation of isoprene from MCM v3.3.1, which includes 611 intermediate species and 1944 chemical reactions, representing the most comprehensive representation of isoprene chemistry currently available. The D-GC and D-GCnew models adopted the default isoprene chemical mechanisms from GEOS-Chem version 14.2.3 and the updated mechanisms developed in this study, respectively. DSMACC used the Kinetic Pre-Processor (KPP) (Sandu and Sander, 2006; Lin et al., 2023) to process kinetics chemical mechanisms. KPP used implicit solver to deal with fast chemical reactions with radicals, making the chemical state in DSMACC sensitive to the radical production rate. Because not all radicals sources was included in DSMACC experiments, the radical production rates were different from the real condition and were more sensitive to NO_X concentrations. Therefore, rather than constraining HO_X concentrations, we created a dummy OH source in DSMACC to produce OH radicals as a constant rate (1.3×10^6 molec cm^{-3} s^{-1})

To quantify glyoxal yields from isoprene, we initialized the model with 1 ppb isoprene for all experiments. we turned off the chemical reactions removing glyoxal in all DSMACC experiments, and the simulation periods are 96 hours, much larger than the lifetime of isoprene. Then the ratio of the final glyoxal concentration and the precursor's initial concentration is the glyoxal yield derived from DSMACC.

Table S1. Observed surface or boundary layer mean glyoxal concentration over land and ocean. Surface glyoxal concentrations are reported unless otherwise noted.

Name	Latitude	Longitude	Period	Hour of Day	Glyoxal (ppt)	Reference
Ocean						
Salt Point	39°N	123°W	Aug Sep 2005	11–14 Local time	20	Seaman et al. (2006)
Carribean Sea	15°N	66°W	Oct 1988	Daily mean	40	Zhou and Mopper (1990)
Sargasso Sea coast	15°N–27°N	94°W–66°W	Oct 1988 Mar 1989	Daily mean	80	Zhou and Mopper (1990)
Tropical Pacific NH	5°N–20°N	133°W–110°W	Jan Mar 2012	Daily mean	32	Coburn et al. (2014)
Tropical Pacific SH	5°S–10°S	110°W–93°W	Jan Mar 2012	Daily mean	43	Coburn et al. (2014)
TP NH aircraft RF12	8.5°N	101.5°W	Jan Feb 2012	Daily mean	25	Volkamer et al. (2015), 0–2 km mean
TP NH aircraft RF17	6°N–7°N	90°W–92°W	Jan Feb 2012	Daily mean	34	Volkamer et al. (2015), 0–2 km mean
Cape Grim	40°S–44°S	140°E–144°E	Aug Sep 2011	Daily mean	7	Lawson et al. (2015)
Chatham Rise	40°S–50°S	175°E–175°W	Feb Mar 2012	Daily mean	23	Lawson et al. (2015)
Tropical Eastern Pacific Ocean	15°S–5°N	85°W–95°W	Nov 2008 Jan 2009	Daily mean	67	Sinreich et al. (2010)
Cape Verde	17°N	25°W	Jun Sep 2014	Daily mean	5.6	Walker et al. (2022)
North Atlantic	40°N–70°N	10°W–10°E	Sep Oct 2017	Daily mean	19	Kluge et al. (2023), 0–2 km mean
Tropical Atlantic	6°S–35°N	40°W–3°E	Aug 2018	Daily mean	44	Kluge et al. (2023), 0–2 km mean
East China Sea	17°N–33°N	122°E–135°E	Mar 2018	Daily mean	75	Kluge et al. (2023), 0–2 km mean
Weddell Sea	43°S–60°S	34°W–75°W	Oct 2019	Daily mean	10	Kluge et al. (2023), 0–2 km mean
Land						
Amazon	12°S–2°N	51°W–68°W	Sep 2014	Daily mean	87	Kluge et al. (2020), 0–2 km mean
Hong Kong	22.217°N	114.25°E	Nov 2020 Feb 2021	10–15 Local time	45	Xu et al. (2023)
Xingtai	37.18°N	114.37°E	Aug 2021	6–18 LT	80	Wang et al. (2019)
Shenzhen	22.55°N	114.60°E	Sep Oct 2019	Daily mean	289	Zhu et al. (2021)
Guangzhou	23°N	113.2°E	Sep Nov 2018	Daily mean	1	Wu et al. (2020)
Hua Guo Shan	22.728°N	112.929°E	Jan 2017	Daily mean	100	Chang et al. (2019)
Mt. Hua	34.48°N	110.08°E	Aug 2020	Daily mean	330	Zhang et al. (2024)
Tazhong	38.97°N	83.66°E	May Jun 2018	Daily mean	210	Geng et al. (2022)
Mt. Hua	34.48°N	110.083°E	Aug 2020	Daily mean	260	Qi et al. (2023)
Shanghai	31.34°N	121.51°E	Jun Aug 2018	Daily mean	162	Guo et al. (2021)
Mt. Fuji-May	32.81°N	130.73°E	May 2016	Daily mean	30	Mitsuishi et al. (2018)
Mt. Fuji-Dec	32.81°N	130.73°E	Dec 2016	Daily mean	5	Mitsuishi et al. (2018)
Sierra Nevada Mountains	38.88°N	120.62°W	Jul 2009	Daily mean	33	DiGangi et al. (2012)
Mexico City	19.5°N	99°W	Apr 2003	Daily mean	270	Volkamer et al. (2007)

(Continued)

Table S1. Observed surface or boundary layer mean glyoxal concentration over land and ocean. (Continued)

Name	Latitude	Longitude	Period	Hour of Day	Glyoxal (ppt)	Reference
Shanghai	31.19°N	121.43°E	May Jun 2021	Daily mean	0.6	Chen et al. (2025), below detection limit
Hefei-MAM	31.78°N	117.2°E	Mar 2018 May 2018	8–17 Local time	230	Hong et al. (2022)
Hefei-JJA	31.78°N	117.2°E	Jun 2018 Aug 2018	8–17 Local time	220	Hong et al. (2022)
Hefei-SON	31.78°N	117.2°E	Sep 2018 Nov 2018	8–17 Local time	220	Hong et al. (2022)
Hefei-DJF	31.78°N	117.2°E	Dec 2018 Feb 2019	8–17 Local time	230	Hong et al. (2022)
Elizabeth-MAM	40.66°N	74.21°W	Mar May 2000 2001	Daily mean	718	Liu et al. (2006)
Elizabeth-JJA	40.66°N	74.21°W	Jun Aug 1999 2000	Daily mean	706	Liu et al. (2006)
Elizabeth-SON	40.66°N	74.21°W	Sep Nov 1999 2000	Daily mean	509	Liu et al. (2006)
Elizabeth-DJF	40.66°N	74.21°W	Dec Feb 1999 2001	Daily mean	448	Liu et al. (2006)
Lhasa	29.63°N	91.02°E	Aug 2000	Daily mean	400	Li et al. (2022)
Madrid-MAM	40.44°N	3.69°E	Mar 2016 May 2016	9 Local time	1410	Benavent et al. (2019)
Madrid-JJA	40.44°N	3.69°E	Jun 2016 Aug 2016	9 Local time	1040	Benavent et al. (2019)
Madrid-SON	40.44°N	3.69°E	Sep 2016 Nov 2016	9 Local time	980	Benavent et al. (2019)
Madrid-DJF	40.44°N	3.69°E	Dec 2016 Jan Feb 2016	9 Local time	1400	Benavent et al. (2019)
Chongqing	29.83°N	107.01°E	Dec 2018 Jan 2019	9–16 Local time	80	Xing et al. (2020)
Montelibretti	42.11°N	12.63°E	Jul Sep 2005	8–16 Local time	440	Possanzini et al. (2007)
Palaiseau-summer	48.71°N	2.21°E	Jul 2009	Daily mean	47	Ait-Helal et al. (2014)
Palaiseau-winter	48.71°N	2.21°E	Jan Feb 2010	Daily mean	158	Ait-Helal et al. (2014)
Rio de Janeiro-May	22.86°N	43.26°W	May 1999	Daytime	201	Grosjean et al. (2002)
Rio de Janeiro-JJA	22.86°N	43.26°W	Jul Aug 2000	Daytime	126	Grosjean et al. (2002)
Rio de Janeiro-SON	22.86°N	43.26°W	Sep Nov 2000	Daytime	99	Grosjean et al. (2002)
Blodgett Forest	38.9°N	120.63°W	Aug Sep 2000	8–21 Local time	27	Spaulding et al. (2003)
Bukit Atur	4.8°N	117.83°E	Apr Jul 2008	Daily mean	335	MacDonald et al. (2012)
Mt. Tai	36.25°N	117.1°E	Jun 2006	Daily mean	188	Kawamura et al. (2013)
Tomakomai Forest	42.73°N	141.52°E	Sep 2003	Daily mean	27	Ieda et al. (2006)
Melbourne-MAM	37.69°S	144.95°E	Mar May 2017 2019	6–17 Local time	164	Fayad et al. (2020)
Melbourne-JJA	37.69°S	144.95°E	Jun Aug 2017 2018	6–17 Local time	139	Fayad et al. (2020)
Melbourne-SON	37.69°S	144.95°E	Sep Nov 2017 2018	6–17 Local time	142	Fayad et al. (2020)
Melbourne-DJF	37.69°S	144.95°E	Dec Feb 2016 2019	6–17 Local time	134	Fayad et al. (2020)
Beijing	39.9°N	116.41°E	Jun 2017	Daily mean	116	Liang et al. (2013)
Los Angeles	34°N	118°W	Jun 2017	Daily mean	103	Washenfelder et al. (2011)
Manitou Forest	39°N	105°W	May Jun 2010	Daily mean	28	Wolfe et al. (2014)
Madison	43°N	89°W	Aug 2010	Daily mean	38	Henry et al. (2012)
Alabama	33°N	87°W	May 2011	Daily mean	29	Kaiser et al. (2016)
SOAS	33°N	87°W	Jun Jul 2013	Daily mean	33	Hettiyadura et al. (2017)
Northern Michigan	45.5°N	84.72°W	Jun Jul 2013	Daily mean	30	Johnson et al. (2008)
Simcoe	43°N	80°W	Jul 2008	Daily mean	500	Aiello et al. (2009)
Wuhan	31°N	114°E	Aug 2021	Daily mean	420	Huang et al. (2023)
Amazon-DJF	2.1°S	59°W	Dec 2019 Feb 2020	Daily mean	70	Donner et al. (2024)
Amazon-MAM	2.1°S	59°W	Mar May 2020	Daily mean	55	Donner et al. (2024)
Amazon-JJA	2.1°S	59°W	Jun Aug 2019	Daily mean	69	Donner et al. (2024)
Amazon-SON	2.1°S	59°W	Sep Nov 2019	Daily mean	80	Donner et al. (2024)

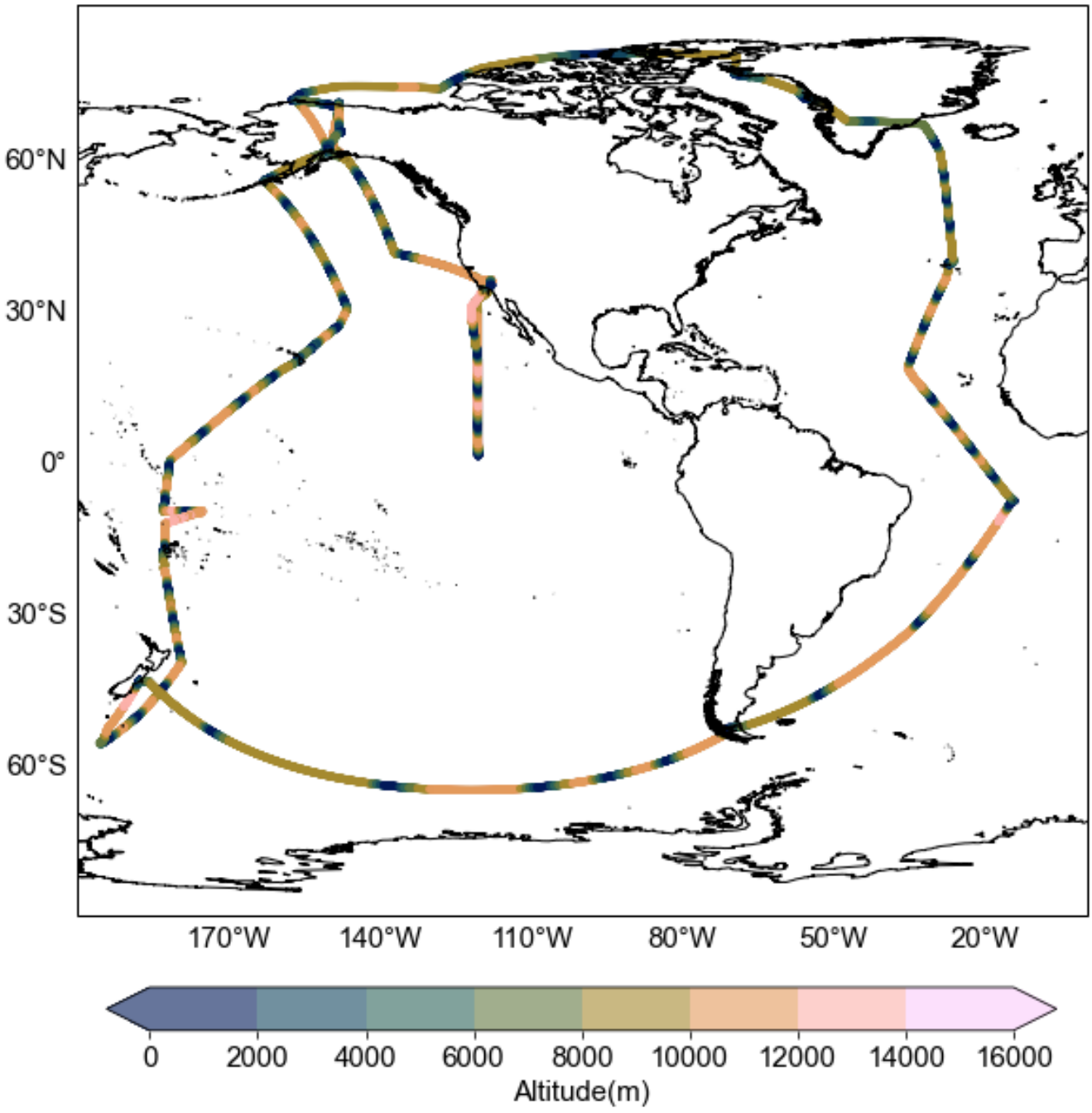

Figure S1. The flight track of the ATom-2 mission.

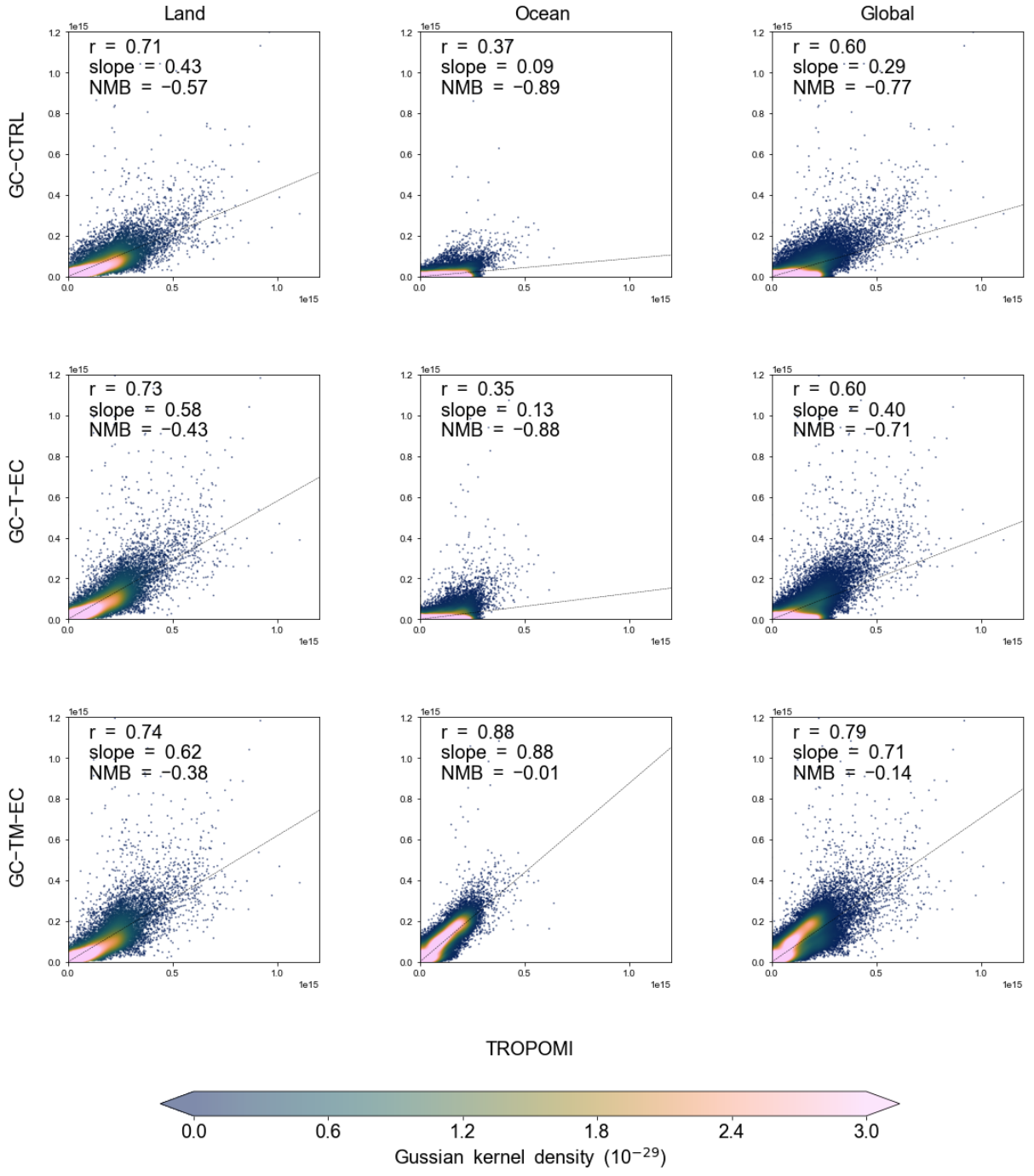

Figure S2. Glyoxal column concentration (molecules cm^{-2}) of TROPOMI observation and GEOS-Chem simulations (GC-CTRL and GC-TM-EC) over land and ocean. Each scatter represents a monthly mean glyoxal column concentration over a $4^{\circ} \times 5^{\circ}$ grid box.

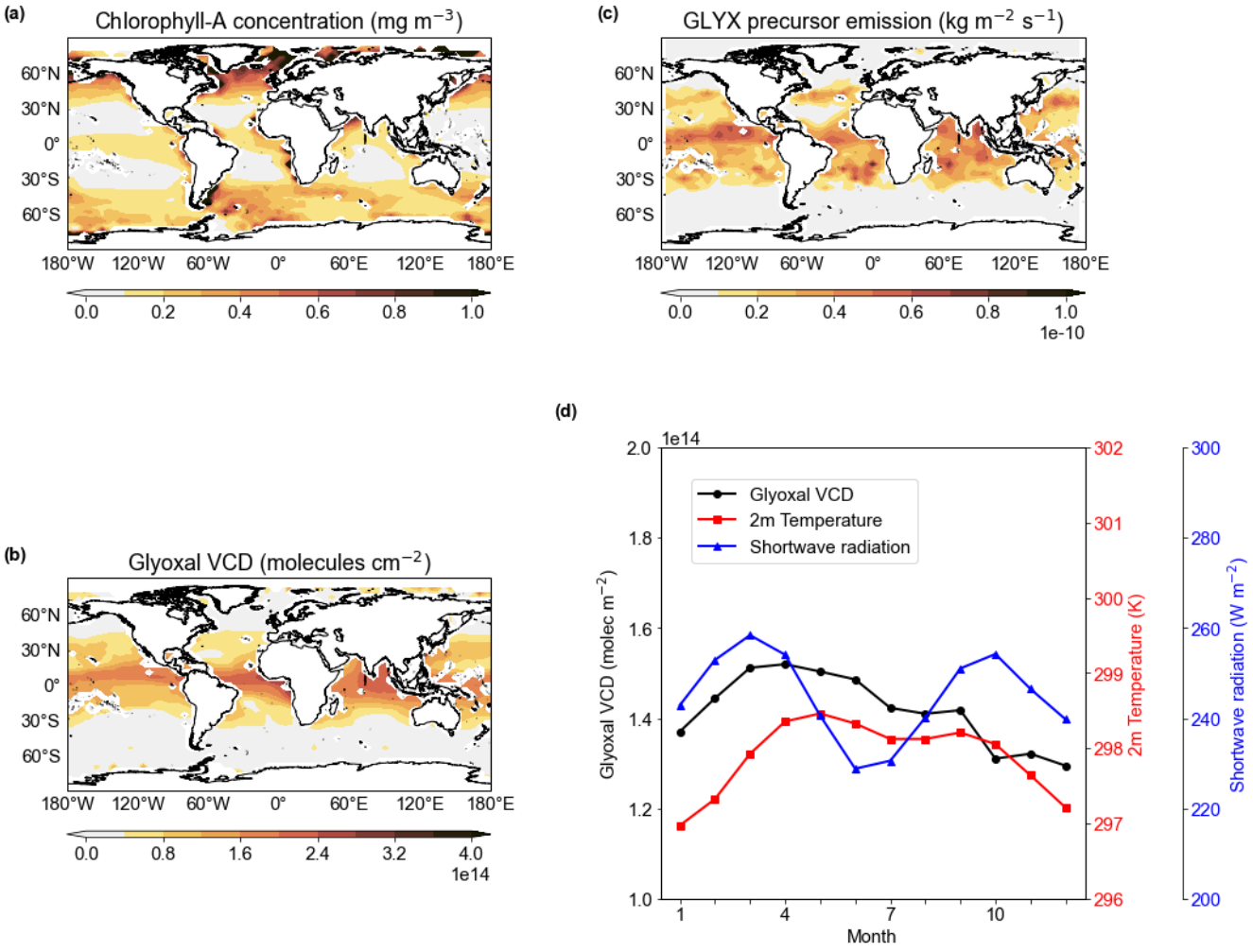

Figure S3. (a) Annual mean chlorophyll-A concentrations in surface sea water retrieved by the MODIS instrument; (b) annual mean TROPOMI-observed glyoxal VCD over the ocean; (c) annual mean emissions of the hypothetical marine precursor of glyoxal as estimated in this study; (d) seasonal variation of TROPOMI-observed glyoxal VCD, 2-m air temperature, and surface downward shortwave radiation flux over the tropical ocean (30° S-30° N).

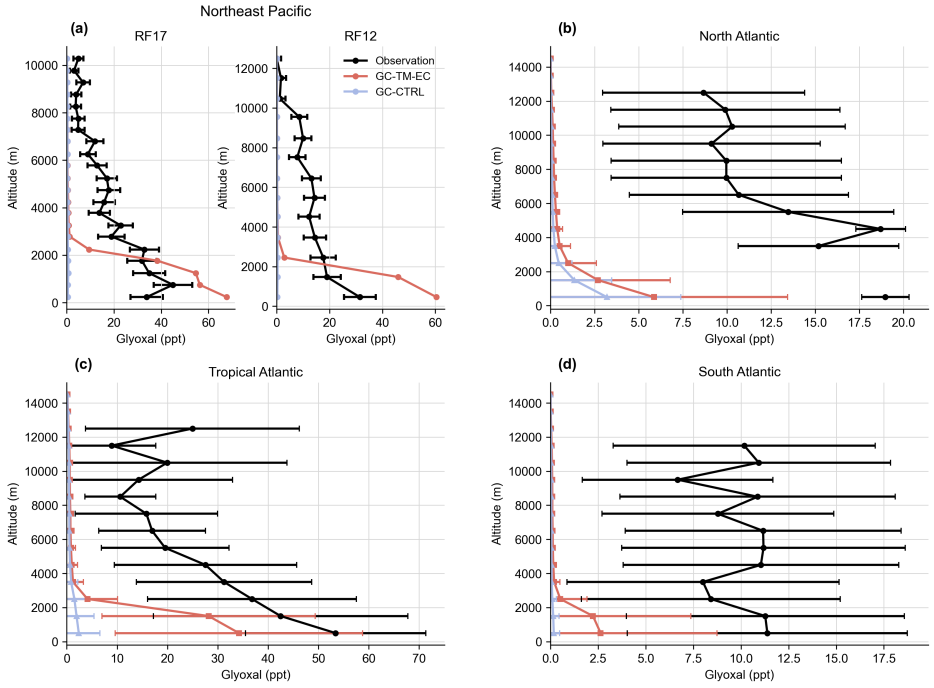

Figure S4. Observed (black) and simulated vertical profiles of glyoxal (a) over the Northeast Pacific during two flights RF17 and RF12 as reported by Volkamer et al. (2015), and over (b) the North Atlantic, (c) the Tropical Atlantic, and (d) the South Atlantic during multiple flights as reported by Kluge et al. (2023). Simulated results from the GC-CTRL (blue) and GC-TM-EC (red) experiments were sampled at the coordinates of the measurements during the month of measurements. Whiskers indicate standard deviations within each vertical layer.

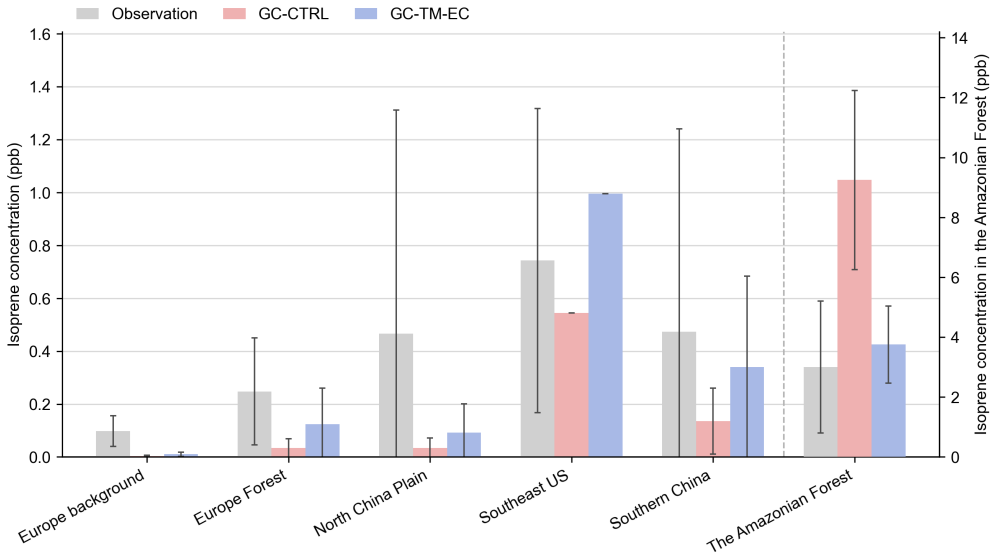

Figure S5. Evaluations of GEOS-Chem simulated surface isoprene concentrations (unit: ppb) against measurements in major source areas of biogenic isoprene: Europe background (Garg et al., 2026), Europe forest (Seco et al., 2011), Amazonian forest (Sun et al., 2025), North China Plain (Zhang et al., 2020), South China (Zhang et al., 2020) and Southeast US forest (Link et al., 2015). The Amazonian forest site is plotted on a separate linear axis because of its much higher concentration range.

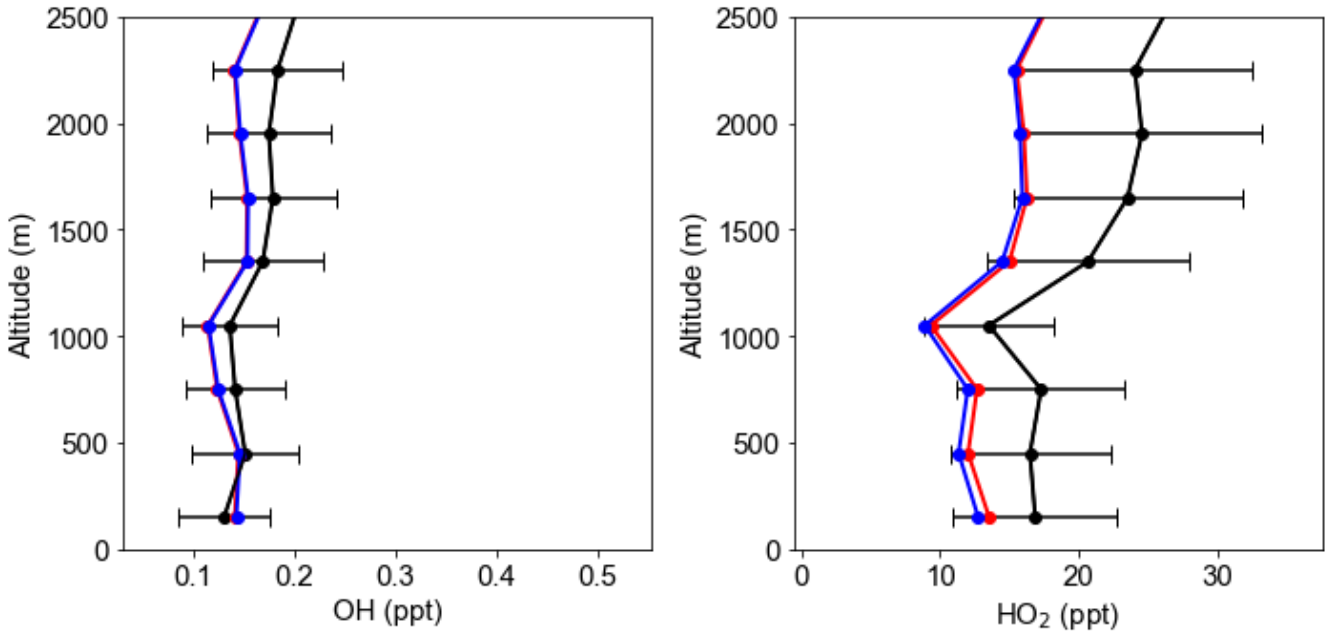

Figure S6. The vertical profiles of ATom-2 aircraft measurements over the tropical ocean (20°S-20°N) and corresponding simulated OH and HO_2 concentration (GC-CTRL in blue; GC-TM-EC in red) within the MBL.

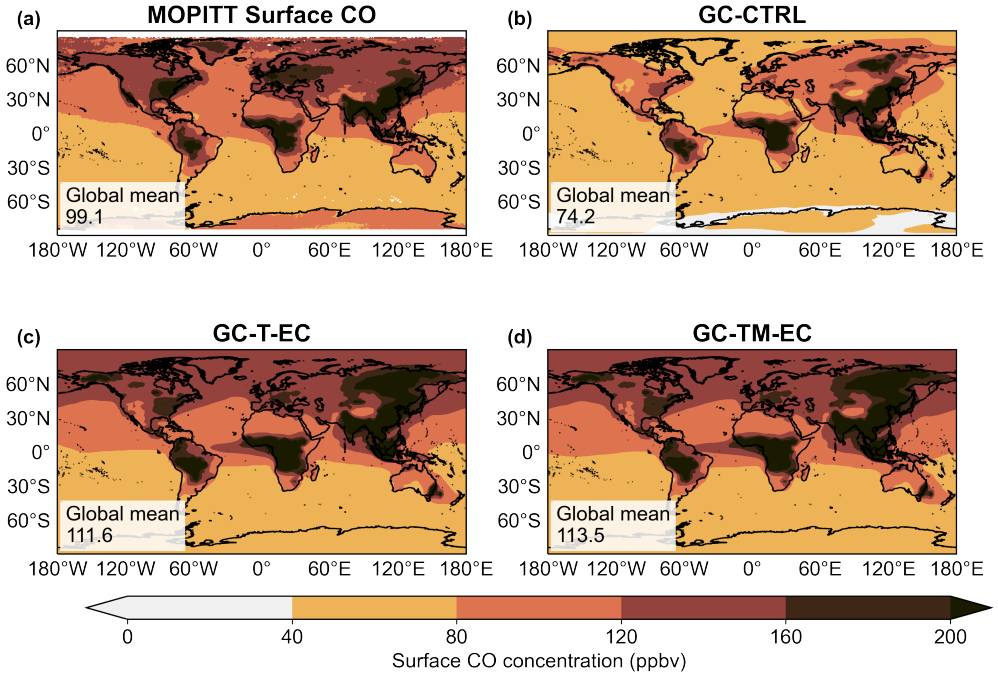

Figure S7. The annual mean (a) MOPITT-retrieved surface CO concentrations and simulated surface CO concentrations in the (b) GC-CTRL, (c) GC-T-EC and (d) GC-TM-EC experiments (unit: ppb) from July 2019 to June 2020. For MOPITT, the annual mean surface CO was derived from the average of the daytime and nighttime retrievals, corresponding to approximately 10:30 and 22:30 local time, respectively.

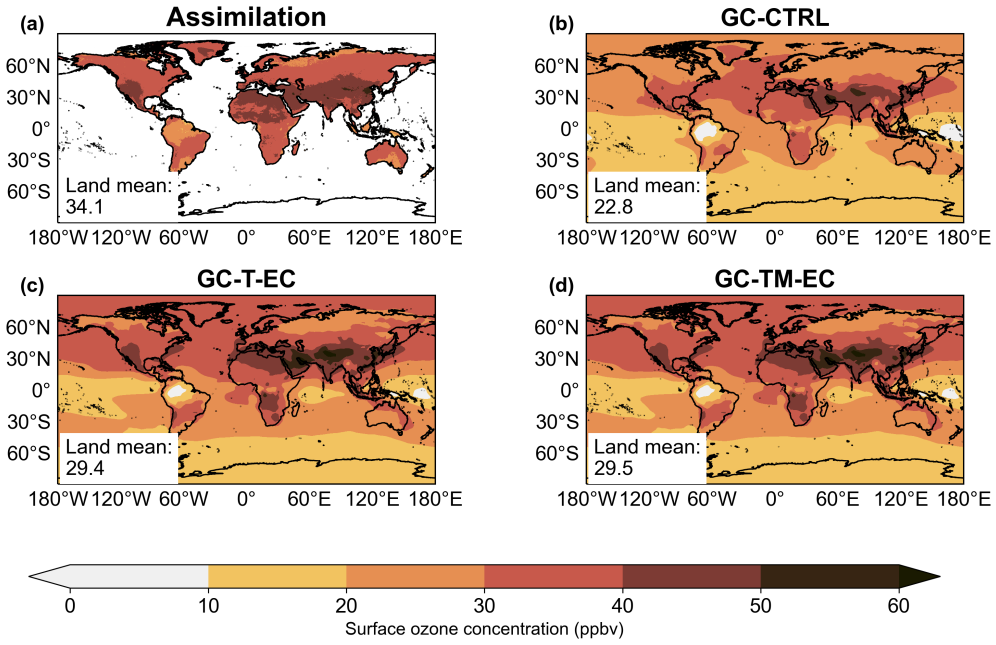

Figure S8. The annual mean (a) assimilated global surface ozone concentrations over land (Wang et al., 2025) and simulated surface ozone concentrations in the (b) GC-CTRL, (c) GC-T-EC and (d) GC-TM-EC experiments (unit: ppb) from July 2019 to June 2020.

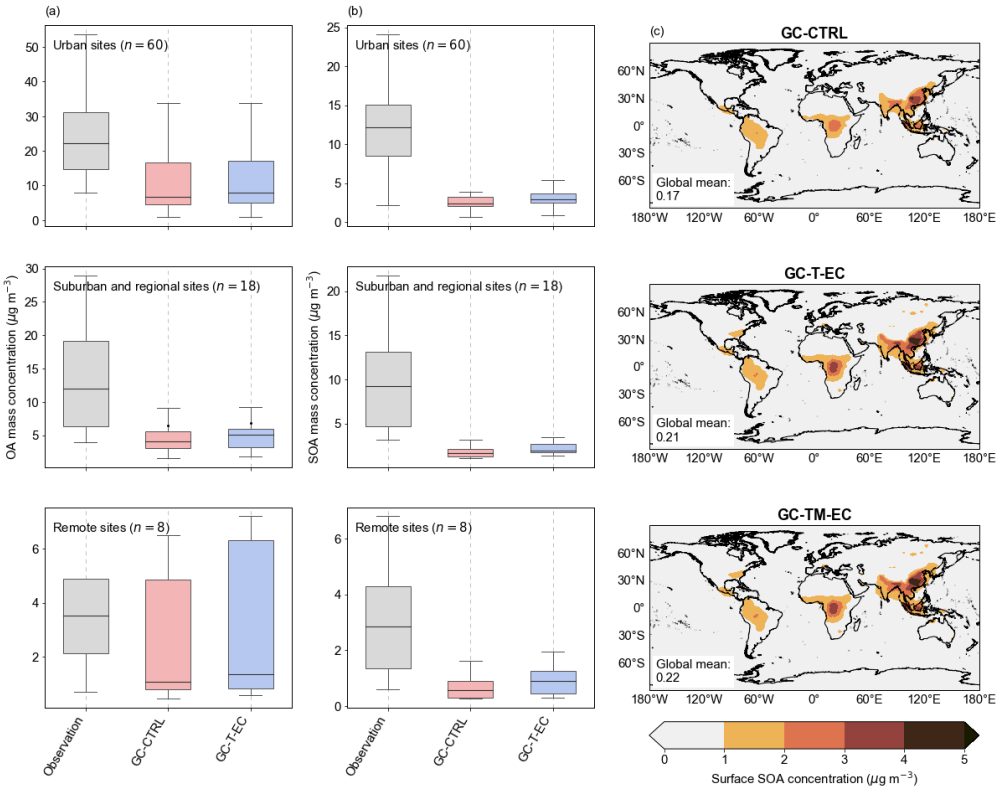

Figure S9. Evaluations of GEOS-Chem simulated (a) OA and (b) SOA against the measurements summarized by Miao et al. (2021) in China. In each boxplot, the horizontal line marks the median, the box represents the interquartile range (25th to 75th percentiles). The whiskers indicate the spread of the corresponding observations and simulations. (c) The simulated annual mean surface SOA concentration in GC-CTRL, GC-T-EC and GC-TM-EC (unit: μg mth) from July 2019 to June 2020.

References

Garg, A., Desservettaz, M., Christodoulou, A., Christoudias, T., Kanawade, V. P., Savvides, C., Vrekoussis, M., Naqui, S., Jokinen, T., Byron, J., Williams, J., Mihalopoulos, N., Liakakou, E., Sciare, J., and Bourtsoukidis, E.: Heat and continental transport shape the variability of volatile organic compounds in the Eastern Mediterranean: insights from multi-year observations and regional modeling, Atmospheric Chemistry and Physics, 26, 2597–2622, https://doi.org/10.5194/acp-26-2597-2026, 2026.

Kluge, F., Hüneke, T., Lerot, C., Rosanka, S., Rotermund, M. K., Taraborrelli, D., Weyland, B., and Pfeilsticker, K.: Airborne glyoxal measurements in the marine and continental atmosphere: comparison with TROPOMI observations and EMAC simulations, Atmospheric Chemistry and Physics, 23, 1369–1401, https://doi.org/10.5194/acp-23-1369-2023, 2023.

Lin, H., Long, M. S., Sander, R., Sandu, A., Yantosca, R. M., Estrada, L. A., Shen, L., and Jacob, D. J.: An Adaptive Auto-Reduction Solver for Speeding Up Integration of Chemical Kinetics in Atmospheric Chemistry Models: Implementation and Evaluation in the Kinetic Pre-Processor (KPP) Version 3.0.0, Journal of Advances in Modeling Earth Systems, 15, e2022MS003 293, https://doi.org/10.1029/2022MS003293, 2023.

Link, M., Zhou, Y., Taubman, B., Sherman, J., Morrow, H., Krintz, I., Robertson, L., Cook, R., Stocks, J., West, M., and Sive, B. C.: A characterization of volatile organic compounds and secondary organic aerosol at a mountain site in the Southeastern United States, Journal of Atmospheric Chemistry, 72, 81–104, https://doi.org/10.1007/s10874-015-9305-5, 2015.

Sandu, A. and Sander, R.: Simulating chemical systems in Fortran90 and Matlab with the Kinetic PreProcessor KPP-2.1, Atmospheric Chemistry and Physics, 6, 187–195, https://doi.org/10.5194/acp-6-187-2006, 2006.

Seco, R., Peñuelas, J., Filella, I., Llusià, J., Molowny-Horas, R., Schallhart, S., Metzger, A., Müller, M., and Hansel, A.: Contrasting winter and summer VOC mixing ratios at a forest site in the Western Mediterranean Basin: the effect of local biogenic emissions, Atmospheric Chemistry and Physics, 11, 13 161–13 179, https://doi.org/10.5194/acp-11-13161-2011, 2011.

Sun, S., Palmer, P. I., Siddans, R., Kerridge, B. J., Ventress, L., Edtbauer, A., Ringsdorf, A., Pfannerstill, E. Y., and Williams, J.: Seasonal isoprene emission estimates over tropical South America inferred from satellite observations of isoprene, Atmospheric Chemistry and Physics, 25, 15 801–15 818, https://doi.org/10.5194/acp-25-15801-2025, 2025.

Volkamer, R., Baidar, S., Campos, T. L., Coburn, S., DiGangi, J. P., Dix, B., Eloranta, E. W., Koenig, T. K., Morley, B., Ortega, I., Pierce, B. R., Reeves, M., Sinreich, R., Wang, S., Zondlo, M. A., and Romashkin, P. A.: Aircraft measurements of BrO, IO, glyoxal, NO_2, H_2O, O_2–O_2 and aerosol extinction profiles in the tropics: comparison with aircraft-/ship-based in situ and lidar measurements, Atmospheric Measurement Techniques, 8, 2121–2148, https://doi.org/10.5194/amt-8-2121-2015, 2015.

Wang, R., Shen, H., Zeng, C., Chen, J., Wang, Y., and Li, Y.: A global land daily 10-km-resolution surface ozone dataset from 2013–2022, Scientific Data, 12, 1710, https://doi.org/10.1038/s41597-025-05990-x, 2025.

Xiong, E., Guo, H., Fu, T.-M., Lyu, X., Wang, Y., Zhou, B., Xia, M., Zou, Z., Yuan, Q., Yang, J., Shek, K. Y., Chen, J., Jiang, T., Tao, W., Zhang, A., Xiang, W., Lee, S., and Wang, T.: Complex impacts of oxygenated volatile organic compounds on radical photochemistry in the background air of Southern China, Submitted, 2025.

Zhang, Y., Zhang, R., Yu, J., Zhang, Z., Yang, W., Zhang, H., Lyu, S., Wang, Y., Dai, W., Wang, Y., and Wang, X.: Isoprene Mixing Ratios Measured at Twenty Sites in China During 2012–2014: Comparison With Model Simulation, Journal of Geophysical Research: Atmospheres, 125, e2020JD033 523, https://doi.org/10.1029/2020JD033523, 2020.

Zou, Z., Chen, Q., Xia, M., Yuan, Q., Chen, Y., Wang, Y., Xiong, E., Wang, Z., and Wang, T.: OH measurements in the coastal atmosphere of South China: possible missing OH sinks in aged air masses, Atmospheric Chemistry and Physics, 23, 7057–7074, https://doi.org/10.5194/acp-23-7057-2023, 2023.